

# Effect of Portal Vein and Hepatic Artery Occlusion on Radiofrequency Ablation: Animal Experiment Comparing MR and Histology Measurements of the Ablation Zones

Akitoshi Inoue<sup>1</sup>  · Norihisa Nitta<sup>1</sup> · Yugo Imai<sup>1</sup> · Kai Takaki<sup>1</sup> · Hiroaki Takahashi<sup>2</sup> · Shinichi Ota<sup>1</sup> · Ken-ichi Mukaisho<sup>3</sup> · Yoshiyuki Watanabe<sup>1</sup>

Received: 2 December 2020 / Accepted: 3 March 2021 / Published online: 6 July 2021

© Springer Science+Business Media, LLC, part of Springer Nature and the Cardiovascular and Interventional Radiological Society of Europe (CIRSE) 2021

## Abstract

**Purpose** This animal experimental study evaluated how hepatic artery and portal vein transient occlusion affects the ablation zone of hepatic radiofrequency ablation (RFA).

**Material and methods** Twenty-one rabbits were divided into three groups of seven each: (1) control, (2) hepatic artery occlusion, and (3) portal vein occlusion by a balloon catheter. For each rabbit, two or three RFA sessions were performed using an electrode needle. Ablation time, temperature around the tip of RFA needle at the end of RFA, ablation volume on fat-suppressed T1-weighted image in the hepatobiliary phase, and coagulative necrosis area on histopathology were measured and compared between the three groups using the Kruskal–Wallis paired Mann–Whitney *U* tests.

**Results** In 43 RFA sessions (group 1, 15; group 2, 14; group 3, 14), mean tissue temperature in group 3 ( $77.0\text{ }^{\circ}\text{C} \pm 7.7\text{ }^{\circ}\text{C}$ ) was significantly higher compared to groups 1 ( $59.2\text{ }^{\circ}\text{C} \pm 18.8\text{ }^{\circ}\text{C}$ ;  $P = 0.010$ ) and 2 ( $67.5\text{ }^{\circ}\text{C} \pm 9.9\text{ }^{\circ}\text{C}$ ;  $P = 0.010$ ). In addition, mean ablation volume and coagulative necrosis in group 3 ( $2.10 \pm 1.37\text{ mm}^3$  and  $0.86 \pm 0.28\text{ mm}^2$ , respectively) were larger compared to groups 1 ( $0.84 \pm 0.30\text{ mm}^3$ ;  $P < 0.001$  and  $0.55 \pm 0.26\text{ mm}^2$ ;  $P = 0.020$ , respectively) and 2

( $0.89 \pm 0.59\text{ mm}^3$ ;  $P = 0.002$  and  $0.60 \pm 0.22\text{ mm}^2$ ;  $P = 0.024$ , respectively).

**Conclusion** Portal vein occlusion potentially boosts tissue temperature, ablation volume, and area of histopathologically proven coagulative necrosis during hepatic RFA in the non-cirrhotic liver.

**Keywords** Radiofrequency ablation · Balloon occlusion · Portal vein · Hepatocellular carcinoma · Liver neoplasms

## Introduction

To achieve complete response with radiofrequency ablation (RFA), the ablation area must adequately cover neoplasms with an adequate margin [1, 2], and  $> 60\text{ }^{\circ}\text{C}$  of tissue temperature should be reached [3, 4]. The ablation area depends on both device and host factors. The heat sink (cooling) effect (perfusion-mediated tissue cooling by blood flow) is a host factor to reduce the ablated margin and tissue temperature in monopolar RFA [5].

Transarterial embolization facilitates larger ablation ranges by reducing the heat sink effect [6] and has favorable disease-free survival in hepatocellular carcinoma [7]. Given the hepatic artery and portal vein supply in the non-cirrhotic liver of 25% and 75% of hepatic blood flow, respectively [8], we hypothesized that compared to hepatic artery occlusion, portal vein occlusion mitigates the heat sink effect more effectively and helps to obtain a larger ablation area and higher tissue temperature in RFA for

✉ Akitoshi Inoue  
akino@belle.shiga-med.ac.jp

<sup>1</sup> Department of Radiology, Shiga University of Medical Science, Seta Tsukinowa-cho, Otsu, Shiga 520-2192, Japan

<sup>2</sup> Department of Radiology, Mayo Clinic, 200 First Street SW, Rochester, MN 55905, USA

<sup>3</sup> Division of Human Pathology, Shiga University of Medical Science, Seta Tsukinowa-cho, Otsu, Shiga 520-2192, Japan

hepatic metastasis in the non-cirrhotic liver. Therefore, this animal experimental study aimed to evaluate the effect of transient hepatic artery and portal vein occlusion on the ablation zone of hepatic RFA.

## Materials and Methods

### Animal Models

This study protocol was approved by the Animal Experimentation Committee of our institute, and all experiments were performed according to its Animal Care Guidelines and ethical standards of practice. Twenty-one female Japanese white rabbits (average weight 2.77 kg; range 2.65–2.9 kg) were acquired from Kitayama Labes Co., Ltd., Japan, and divided them into three groups of seven each: (1) control, (2) hepatic artery occlusion, and (3) portal vein occlusion. The rabbits were fasted for 6 h before experiments. General anesthesia with ketamine hydrochloride (20 mg/kg body weight Ketalar; Daiichi Sankyo, Tokyo, Japan) and dexmedetomidine hydrochloride (0.1 mg/kg body weight Domitor; Zenoac, Fukushima, Japan) was administered intramuscularly. The extremities were fixed to an acryl board in the supine position, and the room temperature was maintained at 25 °C.

### Hepatic Artery Occlusion

The right femoral artery was exposed, and a 4 Fr introducer sheath (Super sheath, length 7 cm; Medikit, Tokyo, Japan) was inserted. Next, a 4 Fr cobra-shaped catheter (Terumo Clinical Supply, Gifu, Japan) was carried to the celiac artery via the introducer sheath, and a 2.1 Fr balloon catheter (LOGOS, length 1050 mm, balloon diameter 3–5 mm, balloon length 12 mm; Piolax, Kanagawa, Japan) was inserted into the proper hepatic artery, and the balloon was inflated to occlude it. To confirm hepatic artery occlusion, angiography using a fluoroscopic system (Plesart 50 DREX-WIN20P fluoroscopic system (Canon Medical Systems, Tochigi, Japan) was performed with a tube voltage of 70 kV and a tube current of 50 mA (Fig. 1A, B).

### Portal Vein Occlusion

After creating an incision in the abdominal wall, the superior mesenteric vein was punctured using a 22-gauge needle (Surflo Flash; Termo, Tokyo, Japan) and a 5 Fr introducer sheath (Super sheath length 7 cm; Medikit) was inserted. Next, a 5.2 Fr balloon catheter (Selecon MP catheter, balloon diameter 9 mm, balloon length 70 mm; Terumo Clinical Supply) was carried to the main portal

vein and the balloon was inflated to occlude it. Finally, venography from the introducer sheath was performed to confirm portal vein occlusion (Fig. 1C, D).

### RFA

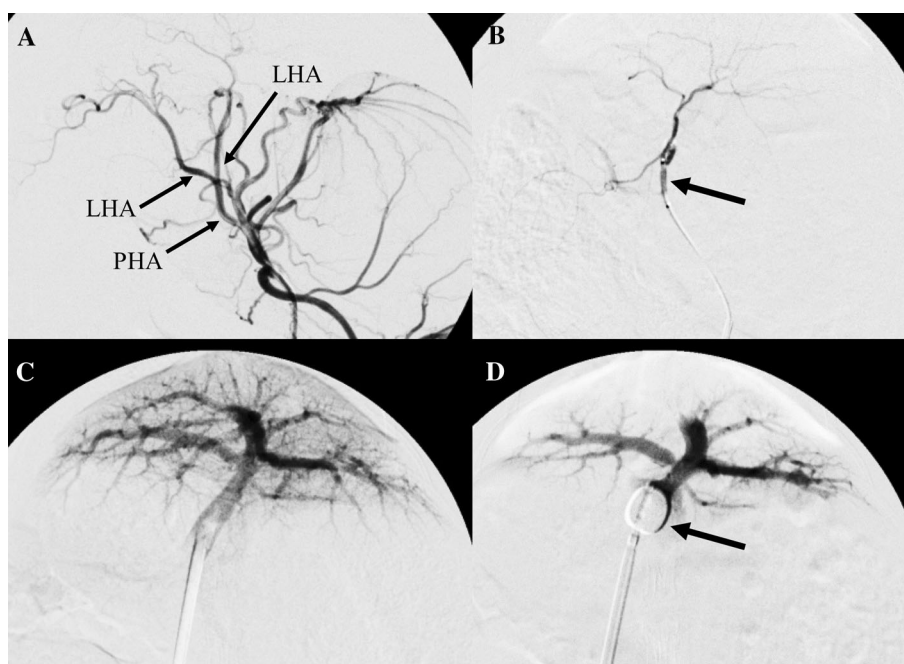
After incision of the abdominal wall at the midline, RFA was performed using the Radionics Cool-tip RF system (RADIONICS, MA, USA) equipped with a 15-cm electrode needle with a 1-cm exposure tip (Cool-tip needle length 15 cm, ablation length 1 cm; Covidien, MA, USA) in impedance control mode by employing a water circulation cooling system. The RFA single-electrode kit was inserted into the left and right lobes of the liver and initiated RFA with a power output of 10 W, gradually raising it by 5 W every 30 s until roll-off by increased impedance. An additional RFA session was performed for the middle of the liver if the distance between the previous two ablation zones was adequate. The ablation time and tissue temperature around the tip at roll-off were recorded. After the RFA sessions, the incised abdominal wall was sutured.

### MRI

MRI was performed using a 3 T scanner (MAGNETOM Verio 3 T, Siemens, Muenchen, Germany) with spine matrix and body matrix coils dedicated to animal experiments 30 min after RFA. Intravenous administration of 0.1 mL/kg of gadoxetate sodium (EOB Primovist; Bayer Yakuhin, Osaka, Japan) was performed in the auricular vein. Next, 15 min after gadoxetate sodium administration (hepatobiliary phase), we obtained fat-suppressed T1WI (FS-T1WI; VIBE) without the breath-gated technique (TR 4.89 ms, TE 2.47 ms, FA 140°, field of view 200 mm, average 1, matrix 256 × 256 mm<sup>2</sup>, gap 0.9 mm, slice thickness 1.0 mm, and scan time 22 s). The total examination time was approximately 20 min.

The shortest distance from the liver surface to the center of the ablation zone was measured on the axial plane on the FS-T1WI because the peripheral area was less affected by the heat sink effect. To define ablation volumes, a medical imaging data set annotation tool (RIL-contour) was used [9]. A radiologist with 12 years of experience segmented the area of low signal intensity and total volume of signal intensity change, which included the low signal intensity and peripheral low signal intensity rims on the FS-T1WI at the hepatobiliary phase (Fig. 2A, B). The volume of identified lesions was automatically calculated using Python version 3.7.

**Fig. 1** Angiogram during hepatic occlusion and portal venous occlusion. **A** Angiogram via the celiac trunk demonstrates the vascular anatomy: the proper hepatic artery (PHA), right hepatic artery (RHA), and left hepatic artery (LHA). **B** Angiogram via a microballoon catheter shows blood flow under the inflated microballoon placed from the PHA (arrow). **C** Portogram via the main trunk of the portal vein showing the venous tree and hepatic parenchymal enhancement. **D** Portogram via the balloon catheter showing blood congestion and a lack of enhancement of the hepatic parenchyma with the inflated microballoon (arrow)



## Histopathology

Immediately after MRI, the rabbits were sacrificed by intravenous administration of 100 mg/kg of pentobarbital sodium (Somnopentyl, Kyoritsu Seiyaku, Tokyo, Japan). The liver was then extracted and stored in 10% formalin for 2 days. Next, it was sliced into 1-cm slices in the axial plane to correspond with the MRI. The samples were embedded in paraffin, cut into 3.5- $\mu$ m-thick sections, and stained with hematoxylin–eosin (H&E).

All pathological slides were converted to virtual slides and reviewed using the NDP.view2 viewer (Hamamatsu Photonics, Shizuoka, Japan). A pathologist with 17 years of experience defined the area involved in coagulative necrosis and peripheral congestion and edema (Fig. 2C, D) [10]. These areas were then converted to binary images using the image manipulation program GIMP, ver.2.10.22 and automatically calculated using Python version 3.7.

## Statistical Analysis

Means, standard deviations, and 95% confidence intervals were calculated for the evaluated parameters. The Kruskal–Wallis test was used for the univariate comparisons of each parameter among the three groups, and the paired Mann–Whitney *U* test with Holm correction was conducted to compare the difference among each group if the Kruskal–Wallis test showed statistical significance. Analysis of covariance (ANCOVA) was used for the multivariable analysis to reveal the independent factors that increased ablation volume or area. Spearman rank correlation

coefficient was used to assess the correlation between ablation volume on MRI and coagulative necrosis on histopathology and the congestion area.  $P < 0.05$  was considered statistically significant. All statistical tests were conducted using R version 4.0.2 (R Foundation for Statistical Computing, Vienna, Austria).

## Results

One rabbit in the control group was excluded because of fusion of two ablation zones, two rabbits in the arterial occlusion group were excluded because of poor liver intake of gadoxetate sodium, and two rabbits in the portal occlusion group were excluded because of unsuccessful portal occlusion. Consequently, a total of 43 RFA sessions were performed, which included 15 sessions in six rabbits in the control group (two sessions in three rabbits and three sessions in three rabbits), 14 sessions in five rabbits in the arterial occlusion group (two sessions in one rabbit and three sessions in four rabbits), and 14 sessions in five rabbits in the portal occlusion group (two sessions in one rabbit and three sessions in four rabbits).

A significant difference was found among the three groups with respect to tissue temperature ( $P = 0.003$ ), total intensity–changed volume ( $P = 0.003$ ), and ablation volume ( $P < 0.001$ ) on MRI, total area of pathology change area ( $P = 0.003$ ), and coagulative necrosis area ( $P = 0.010$ ) (Table 1). Tissue temperature in the portal occlusion group ( $77.0\text{ }^{\circ}\text{C} \pm 7.7\text{ }^{\circ}\text{C}$ ) was significantly higher compared to the control ( $59.2\text{ }^{\circ}\text{C} \pm 18.8\text{ }^{\circ}\text{C}$ ;

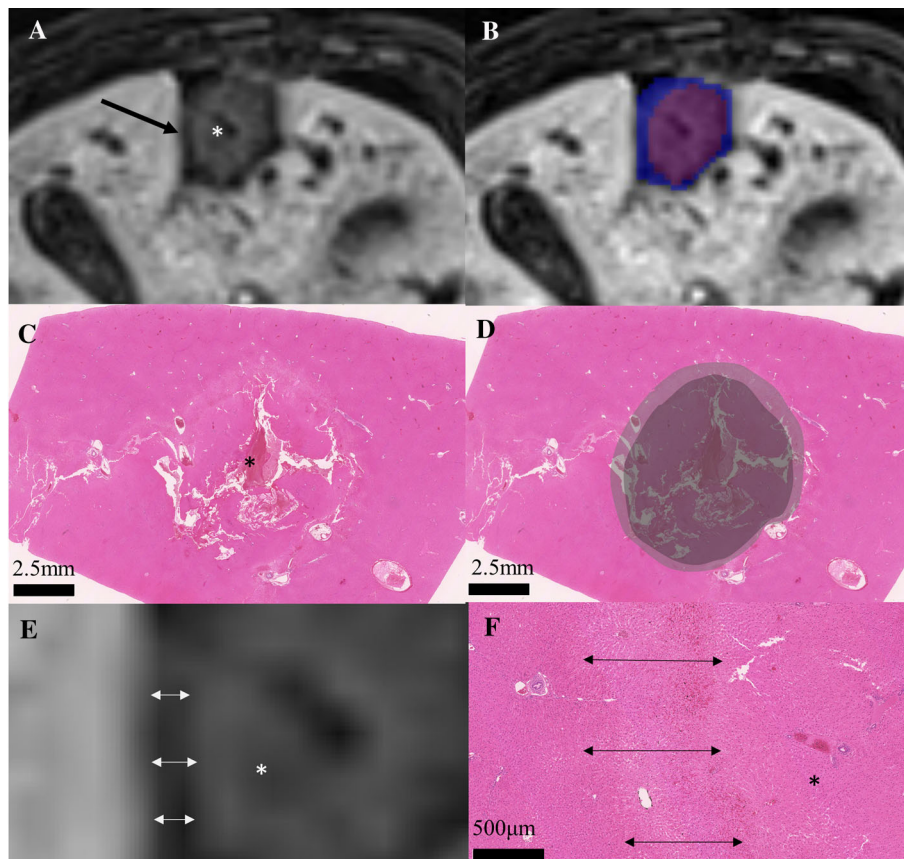


**Fig. 2** Volume measurement on MRI and area measurement on histopathology **A** Ablated hepatic lesion demonstrated a low signal intensity area (\*) surrounded by low signal intensity rim (arrow) on the fat-suppressed T1-weighted image at the hepatobiliary phase. **B** The low signal intensity volume was segmented as ablation volume (purple segmentation), and the volume including the low signal intensity and peripheral low signal intensity rim was segmented as the total volume of signal intensity change (blue segmentation).

Segmentation was performed for every slice with a signal intensity change due to ablation. **C** Ablated lesion around the central needle scar (\*) observed on histopathology (H&E stain). **D** Inner coagulative necrosis area (dark gray) and peripheral edema (light gray) converted to binary data. (e and f) The low signal intensity (\*) and peripheral low intensity signal rim (arrows) on MRI corresponding to coagulative necrosis (\*) and congestion and edema (arrows) on histopathology. H&E, hematoxylin–eosin

$P = 0.010$ ) and hepatic artery occlusion groups ( $67.5 \text{ }^\circ\text{C} \pm 9.9 \text{ }^\circ\text{C}$ ;  $P = 0.010$ ) (Tables 1 and 2). The tissue temperature of the hepatic artery occlusion group was higher than that of the control group, but this was not significant ( $67.5 \pm 9.9$  vs.  $59.2 \pm 18.8 \text{ }^\circ\text{C}$ ;  $P = 0.710$ ). All RFA sessions (15/15) under portal vein occlusion achieved  $> 60 \text{ }^\circ\text{C}$  tissue temperature, whereas in the control and hepatic artery occlusion groups,  $> 60 \text{ }^\circ\text{C}$  tissue temperature was attained in only 66.7% (10/15) and 57.1% (8/15), respectively.

On MRI, total signal intensity change and ablation volumes in the portal vein occlusion group ( $2.81 \pm 1.64$  and  $2.10 \pm 1.37 \text{ cm}^3$ , respectively) were larger than those of the control ( $1.61 \pm 0.53 \text{ cm}^3$ ;  $P = 0.003$  and  $0.84 \pm 0.30 \text{ cm}^3$ ;  $P < 0.001$ , respectively) and hepatic artery occlusion groups ( $1.55 \pm 0.80 \text{ cm}^3$ ;  $P = 0.012$  and  $0.89 \pm 0.59 \text{ cm}^3$ ;  $P = 0.002$ , respectively) (Tables 1 and 2). There was no significant difference in the shortest

distance from the liver surface to the center of ablation zone among the three groups ( $P = 0.290$ ). On histopathology, the total change and coagulative necrosis area in the portal vein occlusion group ( $1.22 \pm 0.28$  and  $0.86 \pm 0.28 \text{ cm}^2$ , respectively) were larger compared with the control ( $0.80 \pm 0.31$ ;  $P = 0.002$  and  $0.55 \pm 0.26 \text{ mm}^2$ ;  $P = 0.020$ , respectively) and hepatic artery occlusion groups ( $0.87 \pm 0.28 \text{ cm}^2$ ;  $P = 0.018$  and  $0.60 \pm 0.22 \text{ cm}^2$ ;  $P = 0.024$ , respectively) (Tables 1 and 2). Ablation volume on MRI and coagulative necrosis area on histopathology in the hepatic artery occlusion group were greater than those in the control group, but these did not reach significance ( $P = 0.683$  and  $0.533$ , respectively).

In ANCOVA, the ablation time and types of occluded vessels independently affected ablation volume ( $F = 4.080$ ;  $P = 0.052$  and  $F = 9.427$ ;  $P = 0.001$ , respectively) and coagulative necrosis ( $F = 4.934$ ,  $P = 0.034$  and  $F = 6.665$ ,  $P = 0.004$ , respectively) (Table 3). Ablation

**Table 1** Means (standard deviations), 95% confidence intervals, and *P*-value for each parameter

	Control	Hepatic artery occlusion	Portal vein occlusion	<i>P</i> -value
<b>RFA parameter</b>				
Ablation time (sec)	173.1 (69.7) 95% CI: 133.2–213.1	126.1 (45.3) 95% CI: 98.9–153.2	148.9 (33.5) 95% CI: 128.9–169.0	0.137
Tissue temperature (°C)	59.2 (18.8) 95% CI: 48.4–70.0	67.5 (9.9) 95% CI: 58.5–70.4	77.0 (7.7) 95% CI: 72.4–81.6	0.003*
The shortest distance from hepatic surface to center of the ablation zone (cm)	8.7 (1.9) 95% CI: 7.6–9.8	8.7 (1.6) 95% CI: 7.8–9.7	10.2 (2.9) 95% CI: 8.5–11.9	0.290
<b>Volume on MRI</b>				
Total volume of signal intensity change (cm <sup>3</sup> )	1.61 (0.53) 95% CI: 1.30–1.91	1.55 (0.80) 95% CI: 1.07–2.03	2.81 (1.64) 95% CI: 1.83–3.79	0.003*
Ablation volume (cm <sup>3</sup> )	0.84 (0.30) 95% CI: 0.67–1.02	0.89 (0.59) 95% CI: 0.54–1.25	2.10 (1.37) 95% CI: 1.27–2.91	< 0.001*
<b>Area on histopathology</b>				
Total area of pathological change (cm <sup>2</sup> )	0.80 (0.31) 95% CI 0.62–0.98	0.87 (0.28) 95% CI: 0.70–1.03	1.22 (0.28) 95% CI: 1.05–1.39	0.003*
Coagulative necrosis (cm <sup>2</sup> )	0.55 (0.26) 95% CI 0.41–0.74	0.60 (0.22) 95% CI: 0.47–0.74	0.86 (0.28) 95% CI: 0.69–1.02	0.010*

95% CI, 95% confidence interval; *SD* standard deviation, *RFA* radiofrequency ablation

\**P* < 0.05 (Kruskal–Wallis test)

**Table 2** *P* values of the intergroup comparison results

	Control versus hepatic artery occlusion	Control versus portal vein occlusion	Hepatic artery occlusion versus portal vein occlusion
<b>RFA parameter</b>			
Tissue temperature (°C)	0.710	0.010*	0.010*
<b>Volume on MRI</b>			
Total volume of signal intensity change (cm <sup>3</sup> )	0.591	0.003*	0.012*
Ablation volume (cm <sup>3</sup> )	0.683	< 0.001*	0.002*
<b>Area on histopathology</b>			
Total area of pathological change (cm <sup>2</sup> )	0.591	0.002*	0.018*
Coagulative necrosis (cm <sup>2</sup> )	0.533	0.020*	0.024*

*RFA* radiofrequency ablation

\**P* < 0.05 (Wilcoxon signed-rank test)

time and ablation volume were correlated ( $\rho = 0.692$ ,  $R < 0.001$ ), and the slope was steeper in the order of portal vein occlusion, hepatic artery occlusion, and control groups (Fig. 3A). Ablation time and coagulative necrosis were also correlated ( $\rho = 0.666$ ,  $R < 0.001$ ), and the slope of the portal vein occlusion group was steeper compared with the control and hepatic artery occlusion groups (Fig. 3B).

## Discussion

This animal experiment investigated how hepatic artery and portal vein occlusion affect the ablation zone as standard reference of MRI as well as histopathology because volume measurement by MRI with a 1 mm thickness provides more detailed three-dimensional information. In the normal rabbit liver, portal vein occlusion by balloon catheter facilitated an increase in the ablation zone on MRI and histopathology as well as tissue temperature in the

**Table 3** Results of the analysis of covariance

	Mean square	F-value	P-value
Ablation volume on MRI			
Ablation time	3,242,117	4.08	0.052*
Procedure	7,489,768	9.427	0.001*
Tissue temperature	19,154	0.0241	0.878
Ablation time–procedure	1,520,210	1.9134	0.165
Ablation time–tissue temperature	2055	0.0026	0.960
Procedure–tissue temperature	258,313	0.3251	0.725
Ablation time–procedure–tissue temperature	171,154	0.2154	0.807
Coagulative necrosis on histopathology			
Ablation time	3246.800	4.934	0.034*
Procedure	4386.400	6.665	0.004*
Tissue temperature	176.700	0.269	0.608
Ablation time–procedure	111.900	0.170	0.844
Ablation time–tissue temperature	650.200	0.988	0.328
Procedure–tissue temperature	309.1	0.470	0.630
Ablation time–procedure–tissue temperature	618.7	0.940	0.401

Ablation time and vascular occlusion procedure (hepatic artery occlusion and portal vein occlusion) independently affects ablation volume on MRI and coagulative necrosis on histopathology, but not tissue temperature

\* $P < 0.05$

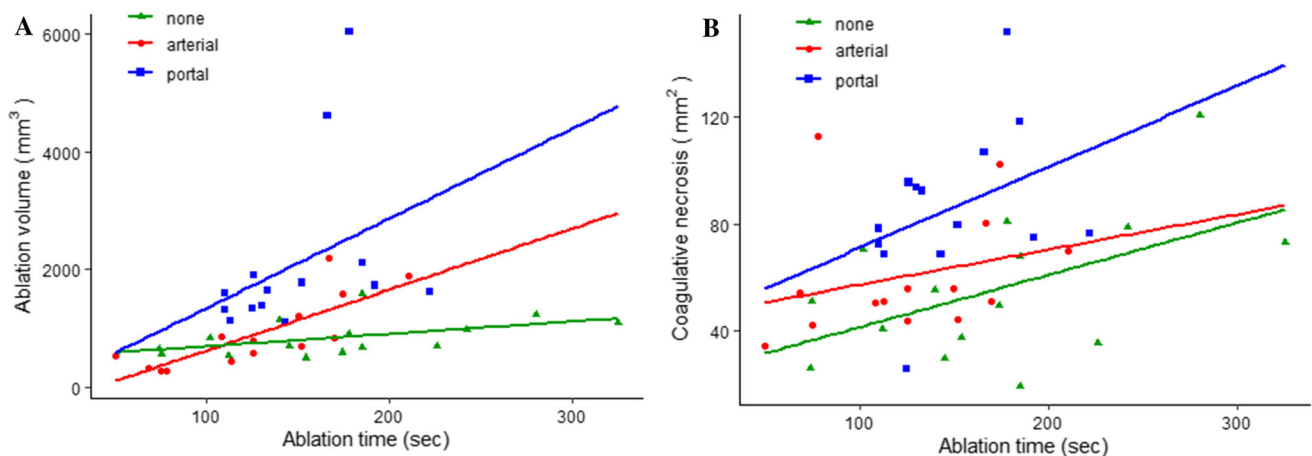


**Fig. 3** Relationship between ablation time and **A** ablation volume on MRI and **B** coagulative necrosis on histopathology in each group. The slope of the regression line of ablation volume on MRI was steeper in the order of portal vein occlusion, hepatic artery occlusion, and

control groups (**A**). The slope of the regression line of coagulative necrosis on histopathology in the portal vein occlusion group was steeper compared with those in the control and hepatic artery occlusion groups (**B**)

hepatic RFA group compared with the hepatic artery occlusion and control groups. MRI was visually evaluated and segmented. Total signal intensity change consisted of low signal intensity and peripheral low signal intensity rim. The low signal intensity and peripheral low signal intensity corresponded to coagulative necrosis and peripheral congestion and edema, respectively (Fig. 2E, F). The hepatic artery occlusion group showed greater ablation volume and coagulative area than the control group, but this was not statistically significant. Total intensity change and ablation

volumes on MRI were correlated with total pathological change, which included congestion and edema ( $\rho = 0.692$ ,  $R < 0.001$ ) and coagulative necrosis area ( $\rho = 0.666$ ,  $R < 0.001$ ), respectively; therefore, ablation volume may be an accurate proxy for post-ablative coagulative necrosis. The ANCOVA results showed that the type of blood vessel maneuvers and ablation time are independent factors in increasing ablation volume. However, the regression between ablation time and ablation zone showed that the increasing rate of ablation area per ablation time was

highest with portal vein occlusion. Portal vein occlusion was shown to be more effective than hepatic artery occlusion and control.

The heat sink effect depended on whether RFA was performed in a peripheral or central location of the liver. Given that the shortest distance between the surface of the liver and the center of the ablation volume was not significantly different between the three groups ( $P = 0.290$ ), the ablation zone may be compared without considering the difference in the degree of the heat sink effect between groups. The coagulative necrosis area was smaller than expected considering an ablation length of 1 cm. However, it is possible that the sampling for the histopathological examination was not obtained at the center of the ablation zone with a maximum diameter.

Tissue temperature is another important outcome of hepatic RFA. A temperature  $> 60$  °C is considered a target to ablate hepatic neoplasms, because above this temperature, rapid protein denaturation occurs [3, 4]. Compared with hepatic arterial occlusion, portal vein occlusion mitigates the heat sink effect and increases tissue temperature, although extremely high temperatures may cause carbonation with insulation, which would subsequently reduce energy deposition.

Most studies investigating the effect of portal vein occlusion on RFA used the Pringle maneuver, which surgically occludes both the hepatic artery and portal vein at the porta hepatis. RFA with the Pringle maneuver produces a larger ablation area compared to RFA without it [11–13]. However, RFA with the Pringle maneuver frequently has adverse effects (portal vein thrombosis, hepatic infarction, and bile duct dilation) several days post-RFA [11, 14]. In contrast, RFA with portal vein occlusion using a balloon catheter shows a higher ablation area and temperature compared to RFA with natural blood flow in the porcine model, with no related complications [15]. While the previous study conventionally measured only the maximum diameter to evaluate the ablation range, we measured the ablation volume on MRI and area on histopathology, with the results consistent with the previous study. Also, the Spearman rank correlation coefficient showed a positive correlation between ablation volume and coagulative necrosis area.

There are several approaches to accessing the portal venous system in the interventional procedure: percutaneous transhepatic [16], percutaneous transsplenic [17], transmesenteric [18], and transjugular intrahepatic approaches [19]. Although we adopted the open-abdominal transmesenteric approach because of simplicity and time saving, the percutaneous transhepatic approach is the most appropriate in terms of convenience and less invasiveness.

This study had several limitations. First, we performed RFA of the non-cirrhotic liver parenchyma to investigate

how portal vein occlusion increases the ablation area by mitigating the heat sink effect. The non-cirrhotic liver parenchyma has 75% and 25% of blood supply from the portal vein and hepatic artery, respectively [8]. In contrast, in liver cirrhosis, the blood supply increases from the hepatic artery and decreases from the portal vein; therefore, the results of this study can be translated to hepatic tumors in a non-cirrhotic liver but not in hepatocellular carcinoma in a cirrhotic liver. Hepatocellular carcinoma (HCC) is fed almost only by the hepatic artery but drains blood into the portal vein [20]. Transarterial chemoembolization is a more reasonable combination with RFA for HCC than portal vein occlusion in terms of the multiplier effect and invasiveness [21, 22]. Second, we did not evaluate delayed adverse events or the presence of arterial and portal thrombosis. However, rabbits are more prone to thrombosis and dissection than humans. Although RFA with the Pringle maneuver causes portal vein thrombosis [11, 14], whether balloon occlusion of the portal vein is safe is unclear. Furthermore, it is uncertain whether simultaneous balloon occlusion of both the hepatic artery and portal vein is safe and effective compared with the Pringle maneuver. Third, the number of rabbits included was small, although it was the minimum sample size required to comply with animal ethics. Fourth, gadoxetate sodium administration shortly after RFA is not recommended clinically although it was performed in the current study to measure ablation volume more precisely. Finally, this study investigated the effect of portal vein occlusion during RFA. The effect of portal vein occlusion during multipolar RFA or microwave ablation, which are the devices most commonly used, was not studied.

## Conclusion

Portal vein occlusion is potentially helpful in obtaining a higher tissue temperature and a larger ablation volume in hepatic RFA for the non-cirrhotic liver.

**Acknowledgment** The authors would like to thank Enago ([www.enago.jp](http://www.enago.jp)) for the English language review

**Funding** The study was not supported by any funding.

## Declarations

**Conflict of interest** The authors declare that they have no conflict of interest.

**Ethical Statement** This study protocol was approved by the Animal Experimentation Committee of our institute, and all experiments were performed according to its Animal Care Guidelines.

**Consent for Publication** All authors agreed the publication of this research.

## References

1. Takeyama N, Mizobuchi N, Sakaki M, Shimosuma Y, Munchika J, Kajiwara A, et al. Evaluation of hepatocellular carcinoma ablative margins using fused pre- and post-ablation hepatobiliary phase images. *Abdom Radiol (NY)*. 2019;44(3):923–35. <https://doi.org/10.1007/s00261-018-1800-0>.
2. Fukuda K, Mori K, Hasegawa N, Nasu K, Ishige K, Okamoto Y, et al. Safety margin of radiofrequency ablation for hepatocellular carcinoma: a prospective study using magnetic resonance imaging with superparamagnetic iron oxide. *Jpn J Radiol*. 2019;37(7):555–63. <https://doi.org/10.1007/s11604-019-00843-1>.
3. Nikfarjam M, Muralidharan V, Christophi C. Mechanisms of focal heat destruction of liver tumors. *J Surg Res*. 2005;127(2):208–23. <https://doi.org/10.1016/j.jss.2005.02.009>.
4. Chu KF, Dupuy DE. Thermal ablation of tumours: biological mechanisms and advances in therapy. *Nat Rev Cancer*. 2014;14(3):199–208. <https://doi.org/10.1038/nrc3672>.
5. Kim SK, Rhim H, Kim YS, Koh BH, Cho OK, Seo HS, et al. Radiofrequency thermal ablation of hepatic tumors: pitfalls and challenges. *Abdom Imaging*. 2005;30(6):727–33. <https://doi.org/10.1007/s00261-005-0304-x>.
6. Duan X, Zhou G, Han X, Ren J, Zheng C, Liang H, et al. Radiofrequency ablation combined with transcatheter therapy in rabbit VX2 liver tumors: effects and histopathological characteristics. *Acta Radiol*. 2015;56(1):87–96. <https://doi.org/10.1177/0284185113520266>.
7. Yamakado K, Nakatsuka A, Takaki H, Yokoi H, Usui M, Sakurai H, Isaji S, Shiraki K, Fuke H, Uemoto S, Takeda K. Early-stage hepatocellular carcinoma: radiofrequency ablation combined with chemoembolization versus hepatectomy. *Radiology*. 2008;247(1):260–6.
8. Carneiro C, Brito J, Bilreiro C, Barros M, Bahia C, Santiago I, et al. All about portal vein: a pictorial display to anatomy, variants and physiopathology. *Insights Imaging*. 2019;10(1):38. <https://doi.org/10.1186/s13244-019-0716-8>.
9. Philbrick KA, Weston AD, Akkus Z, Kline TL, Korfiatis P, Sakinis T, et al. RIL-Contour: a medical imaging dataset annotation tool for and with deep learning. *J Digit Imaging*. 2019;32(4):571–81. <https://doi.org/10.1007/s10278-019-00232-0>.
10. Wright AS, Sampson LA, Warner TF, Mahvi DM, Lee FT Jr. Radiofrequency versus microwave ablation in a hepatic porcine model. *Radiology*. 2005;236(1):132–9.
11. Kim SK, Lim H, Ryu JA, Choi D, Lee WJ, Lee JY, Lee JH, Sung YM, Cho EY, Hong SM, Kim JS. Radiofrequency ablation of rabbit liver in vivo: effect of the Pringle maneuver on pathologic changes in liver surrounding the ablation zone. *Korean J Radiol*. 2004;5(4):240–9.
12. Frich L, Mala T, Gladhaug IP. Hepatic radiofrequency ablation using perfusion electrodes in a pig model: effect of the Pringle manoeuvre. *Eur J Surg Oncol*. 2006;32(5):527–32. <https://doi.org/10.1016/j.ejso.2006.02.021>.
13. Chinn SB, Lee FT Jr, Kennedy GD, Chinn C, Johnson CD, Winter TC 3rd, Warner TF, Mahvi DM. Effect of vascular occlusion on radiofrequency ablation of the liver: results in a porcine model. *AJR Am J Roentgenol*. 2001;176(3):789–95.
14. Ng KK, Lam CM, Poon RT, Shek TW, Fan ST, Wong J. Delayed portal vein thrombosis after experimental radiofrequency ablation near the main portal vein. *Br J Surg*. 2004;91(5):632–9. <https://doi.org/10.1002/bjs.4500>.
15. Goldberg SN, Hahn PF, Tanabe KK, Mueller PR, Schima W, Athanasoulis CA, et al. Percutaneous radiofrequency tissue ablation: does perfusion-mediated tissue cooling limit coagulation necrosis? *J Vasc Interv Radiol*. 1998;9(1):101–11. [https://doi.org/10.1016/s1051-0443\(98\)70491-9](https://doi.org/10.1016/s1051-0443(98)70491-9).
16. Luo J, Yan Z, Wang J, Liu Q, Qu X. Endovascular treatment for nonacute symptomatic portal venous thrombosis through intrahepatic portosystemic shunt approach. *J Vasc Interv Radiol*. 2011;22(1):61–9. <https://doi.org/10.1016/j.jvir.2010.07.028>.
17. Chu HH, Kim HC, Jae HJ, Yi NJ, Lee KW, Suh KS, et al. Percutaneous transsplenic access to the portal vein for management of vascular complication in patients with chronic liver disease. *Cardiovasc Intervent Radiol*. 2012;35(6):1388–95. <https://doi.org/10.1007/s00270-011-0311-y>.
18. Fukuhara S, Ohira M, Chosa K, BaBa Y, Hamaoka M, Tanimine N, et al. Obliteration of a portosystemic shunt by hybrid interventional radiology using a transmesenteric approach under minilaparotomy after liver transplantation: a case report. *Transpl Proc*. 2020;52(9):2762–6. <https://doi.org/10.1016/j.transproceed.2020.06.014>.
19. Carnevale FC, Santos AC, Tannuri U, Cerri GG. Hepatic veins and inferior vena cava thrombosis in a child treated by transjugular intrahepatic portosystemic shunt. *Cardiovasc Intervent Radiol*. 2010;33(3):627–30. <https://doi.org/10.1007/s00270-009-9647-y>.
20. Matsui O, Kobayashi S, Sanada J, Kouda W, Ryu Y, Kozaka K, et al. Hepatocellular nodules in liver cirrhosis: hemodynamic evaluation (angiography-assisted CT) with special reference to multi-step hepatocarcinogenesis. *Abdom Imaging*. 2011;36(3):264–72. <https://doi.org/10.1007/s00261-011-9685-1>.
21. Ikeda M, Kudo M, Aikata H, Nagamatsu H, Ishii H, Yokosuka O, et al. Transarterial chemoembolization with miriplatin versus epirubicin for unresectable hepatocellular carcinoma: a phase III randomized trial. *J Gastroenterol*. 2018;53(2):281–90. <https://doi.org/10.1007/s00535-017-1374-6>.
22. Inoue A, Ota S, Takaki K, Imai Y, Sato S, Watanabe S, et al. Change in hepatic hemodynamics assessed by hepatic arterial blood pressure and computed tomography during hepatic angiography with the double balloon technique. *Jpn J Radiol*. 2019;37(6):487–93. <https://doi.org/10.1007/s11604-019-00836-0>.

**Publisher's Note** Springer Nature remains neutral with regard to jurisdictional claims in published maps and institutional affiliations.